International Journal of Nanomedicine

Dovepress
open access to scientific and medical research

Open Access Full Text Article

ORIGINAL RESEARCH

In vivo Preclinical Tumor-Specific Imaging of Superparamagnetic Iron Oxide Nanoparticles Using Magnetic Particle Imaging for Cancer Diagnosis

Sang-Jin Park[1,*], Seung Ro Han[2,3,*], Yun Hee Kang[2,3,*], Eun-Jin Lee[1], Eu-Gene Kim[1], Hyobong Hong[4], Jae-Chan Jeong[4], Myung-Shin Lee[2,3], Seung-Hoon Lee[2,5], Dae-Yong Song[1]

[1]Department of Anatomy and Neuroscience, Eulji University School of Medicine, Daejeon, Korea; [2]Eulji Biomedical Science Research Institute, Eulji University School of Medicine, Daejeon, Korea; [3]Department of Microbiology and Immunology, Eulji University School of Medicine, Daejeon, Korea; [4]Artifcial Intelligence Research Laboratory, Electronics and Telecommunications Research Institute (ETRI), Daejeon, Korea; [5]Department of Neurosurgery, Eulji University School of Medicine, Daejeon, Korea

*These authors contributed equally to this work

Correspondence: Seung-Hoon Lee, Department of Neurosurgery, Eulji University School of Medicine, Daejeon, Korea, Tel +82-42-259-1612, Fax +82-42-259-1669, Email nslsh@eulji.ac.kr; Dae-Yong Song, Department of Anatomy and Neuroscience, Eulji University School of Medicine, Daejeon, Korea, Tel +82-42-259-1622, Fax +82-42-259-1669, Email dysong@eulji.ac.kr

Purpose: Magnetic particle imaging (MPI) is an emerging radiation-free, non-invasive three-dimensional tomographic technology that can visualize the concentrations of superparamagnetic iron oxide nanoparticles (SPIONs). To verify the applicability of the previously proposed point-of-care testing MPI (PoCT-MPI) in medical diagnosis and therapeutics, we imaged SPIONs in animal tumor models.

Methods: CT26 or MC38 mouse colon carcinoma cells (2×10^6 cells) were subcutaneously injected into the right flank of BALB/c mice. SPIONs were either injected directly into the tumor lesions in the intratumoral group or through tail veins in the intravenous group. CT26 and MC38 tumor models were examined both intratumorally and intravenously to confirm the biological availability of SPIONs using PoCT-MPI.

Results: Signals were observed in the tumor lesions from day 1 to day 7. This is the first study to successfully image the pathological region and show the biodistribution of SPIONs in CT26 tumor models using the recently developed PoCT-MPI technology. Furthermore, MC38 tumor models were examined, resulting in similar images to those of the CT26 tumor model in both intratumoral and intravenous groups.

Conclusion: The present study demonstrates the biological applicability of PoCT-MPI, which promises to be a powerful diagnostic and therapeutic technique in biomedical imaging.

Keywords: colon cancer, syngeneic mouse tumor model, point-of-care testing MPI, diagnostics

Introduction

Magnetic particle imaging (MPI) was first proposed in 2001 by the Royal Philips Research Lab in Hamburg, Germany, and imaging technology using MPI was first published in the literature in 2005.[1] MPI is a new non-invasive, radiation-free tomographic technique in medical diagnosis and therapy.[2,3] At the 2013 World Molecular Imaging Congress (WMIC), Bruker Biospin announced the production of the world's first commercial MPI system, a preclinical imaging scanner.[4] The MPI scanner can create three-dimensional (3D) images by detecting superparamagnetic iron oxide nanoparticles (SPIONs) that are administered into the body.[5] Unlike traditional imaging methods, such as magnetic resonance imaging (MRI), X-ray, and computed tomography (CT), MPI is not a structural imaging technique. Instead, it is a tracer imaging system similar to positron emission tomography (PET) and single-photon emission computed tomography (SPECT).[6]

Received: 27 April 2022
Accepted: 21 August 2022
Published: 26 August 2022

The enormous potential of MPI systems for biomedical research has been demonstrated in several studies, including applications in real-time in vivo monitoring,[7] disease diagnosis, disease progression prediction, drug delivery, targeted cancer immunotherapy, and hyperthermia therapy.[8,9] Recently, in vivo studies have also demonstrated the applicability of MPI scanners in vascular imaging,[10] oncology,[11,12] and cell tracking.[13] Indeed, the exceptional ability to obtain high temporal-spatial resolution in vivo[12] allows for novel applications of MPI by tracking and quantifying SPIONs.[7,13] SPIONs are a type of magnetic nanoparticle that exhibit magnetic properties in the presence of an external magnetic field. Due to their high magnetic properties and sensitivity, SPIONs have been proposed as a material for cancer imaging, diagnosis, and therapy, as well as for drug delivery.[14–17] For example, Yang et al reported that the resolution of MR images was significantly improved when SPIONs were used as a contrast agent by conjugating them with Her-2/neu antibody for the detection of HER2/neu-positive breast cancer.[18] Also, since SPIONs are one of the materials that can selectively induce heat by an external alternating magnetic field, considerable research interest has been focused on the application of hyperthermia.[8,9] Therefore, multifunctional SPIONs can be developed by incorporating various functional materials, and this process enables simultaneous multimodal diagnosis and therapy, which is known as theranostics. Siddique and Chow have provided an in-depth review of recent advances in biomedical imaging and cancer treatment utilizing magnetic nanomaterials, including SPIONs.[19,20]

In our previous studies, we measured free radicals in test-tube samples using one-dimensional (1D) MPI—a modification of the initial basic model—and further suggested the possibility of its application to bio-specimens.[21] Subsequently, two-dimensional (2D) MPI technology was reported to scan sliced tissue to obtain 2D images and 3D modeling of specific disease areas using antibody-conjugated SPIONs in an animal model of ischemia.[22] Furthermore, in vivo visualization of SPIONs was confirmed using point-of-care testing MPI (PoCT-MPI) technology, a novel 3D magnetic particle imaging system based on frequency mixing.[23] Hence, in the current study, we sought to demonstrate the biological and medical utility of PoCT-MPI in cancer diagnosis using CT26 and MC38 syngeneic mouse tumor models.

Materials and Methods

Animals

Adult male BALB/c mice (n = 33; 15 for PoCT-MPI scan, 18 for biodistribution) weighing 19–22 g and female C57BL/6 mice (n = 12 for PoCT-MPI scan and histological examination) weighing 16–18 g were purchased from SamTako Bio Korea (Osan, Korea). They were housed at a constant room temperature (20–22 °C) with a 12:12-h light-dark cycle and provided ad libitum access to food and water. All experimental procedures were performed in accordance with the National Institutes of Health Guide for the Care and Use of Laboratory Animals (NIH Publication No. 80–23, revised 1996), and they were approved by the Eulji University Institutional Animal Care and Use Committee (EUIACUC-19-24, approval date: December 18, 2019).

Superparamagnetic Iron Oxide Nanoparticles (SPIONs)

We successfully identified and validated commercially available SPIONs that were most suitable for PoCT-MPI (Table 1). Dextran-based magnetic nanoparticles, Synomag-D (product no. 104–00-501, Micromod, Rostock,

Table 1 List of the SPIONs Tested in This Study

Nanoparticles	Company (City, Country)	Trade Name	Particle Size	Coating	Iron Concentration
Iron oxide	Chemicell (Berlin, Germany)	UC/A	50 nm	X	10 mg/mL
Iron oxide	Chemicell (Berlin, Germany)	FluidMAG-amine	100 nm	Dextran	No Information
Iron oxide	Chemicell (Berlin, Germany)	FluidMAG-carboxyl	100 nm	Dextran	No Information
Iron oxide	Micromod (Rostock, Germany)	Synomag-D	50 nm	Dextran	10 mg/mL
Iron oxide	Micromod (Rostock, Germany)	Nanomag-D-spio	20, 50, 100 nm	Dextran	2.5 mg/mL

Abbreviation: SPION, Superparamagnetic iron oxide nanoparticles.

Germany) were employed as they exhibit excellent properties as a tracer for PoCT-MPI. Synomag-D is a 50 nm dextran-coated SPION with an iron concentration of 10 μg/μL and a solid concentration of 25 μg/μL.

PoCT-MPI Scan

To obtain a sinogram, electromagnetic field exposure was conducted for 5 s at 20° and rotated nine times. To measure the sensitivity, test tubes containing various amounts of SPIONs from 5 to 50 μg (Fe) were loaded in the PoCT-MPI and visualized to reconstruct images. For PoCT-MPI, the mice were anesthetized with ketamine (14 mg/kg body weight; Yuhan Co., Seoul, Korea) and xylazine (1.6 mg/kg body weight; Bayer Korea, Seoul, Korea) intraperitoneally. Next, the experimental animals were loaded on the PoCT-MPI stage and scanned at 3 mm intervals. A total of 30 sinograms were acquired, and 3D images were obtained using the Radon transform. The conversion program was generated using MATLAB (MathWorks Inc., Natick, MA, USA).

Syngeneic Mouse Tumor Model

Five-week-old male BALB/c mice and five-week-old female C57BL/6 mice were used as animal models to generate tumors. The CT26 and MC38 mouse colon carcinoma cell lines were purchased from the American Type Culture Collection (ATCC, Manassas, VA, USA), preserved, and cultivated at the anatomy laboratory at Eulji University. The cell lines were grown as a monolayer in Dulbecco's modified Eagle's medium (DMEM; Sigma-Aldrich, St Louis, MO, USA) containing 10% fetal bovine serum (FBS; Sigma-Aldrich) and 1% L-glutamine. Full-grown monolayer cultures were trypsinized for 15 min (0.25% trypsin-EDTA), harvested, and passaged several times for expansion. Following the growth and expansion of the cell line in vitro, trypsinized cells were harvested, washed, counted using the trypan blue dye exclusion method, and cell density was adjusted to 2.0×10^6. Viable tumor cells in 0.2 mL phosphate-buffered saline (PBS) were inoculated subcutaneously into the right flanks of 11 BALB/c mice and 9 C57BL/6 mice. As negative controls of tumor growth, 0.2 mL PBS was inoculated subcutaneously into the right flanks of 4 BALB/c mice and 3 C57BL/6 mice. Thereafter, body weight was measured every seven days. A tumor size check was initiated on day 5 when the tumor volume reached ~10 mm^3. Tumor diameter was measured using an electronic caliper every 3 d, and tumor volume was determined using the following Equation (1):

$$V(mean\ tumor\ volume) = \frac{A \times B^2}{2} \quad (1)$$

where A and B are the long and short axis lengths, respectively.

Intratumoral Injection Model

The SPIONs in the tumor area were scanned using PoCT-MPI in a time-dependent manner. Direct intratumoral delivery of SPIONs was initiated 14 days after CT26 or MC38 challenge, when the tumor diameter was approximately 200 mm^3. Subsequently, SPIONs (200 μg [Fe]) were injected directly into the tumor site. Thereafter, the SPIONs present in the tumor were scanned using PoCT-MPI at 1 h, 4 h, 1 d, and 2 d following CT26 injection (Figure 1), or on day 1, 3, and 5 after MC38 injection (Figure S1).

Intravenous Injection Model

Experiments were conducted to assess whether SPIONs administered through the tail vein accumulated at the tumor sites. The intravenous injection model has been established to measure systemic solid tumors, which are otherwise difficult to access for direct intratumoral injection of SPIONs, using PoCT-MPI. The CT26 tumor-bearing mice were scanned using PoCT-MPI 4 h after intravenous administration of SPIONs (600 μg [Fe]) on day 18 following CT26 tumor inoculation. The tumors were scanned using PoCT-MPI at 1, 2, 3, 4, 7, and 18 d after intravenous administration of SPIONs (1.2 mg [Fe]) on day 21 following CT26 transplantation (Figure 1). In addition, the MC38 tumor-bearing mice were scanned using PoCT-MPI at 4 h, 1 d, 3 d, and 5 d after intravenous SPION administration (1.2 mg [Fe]) and on day 14 following MC38 tumor inoculation (Figure S1). Animals injected with the vehicle (PBS without SPIONs) were used as a negative control.

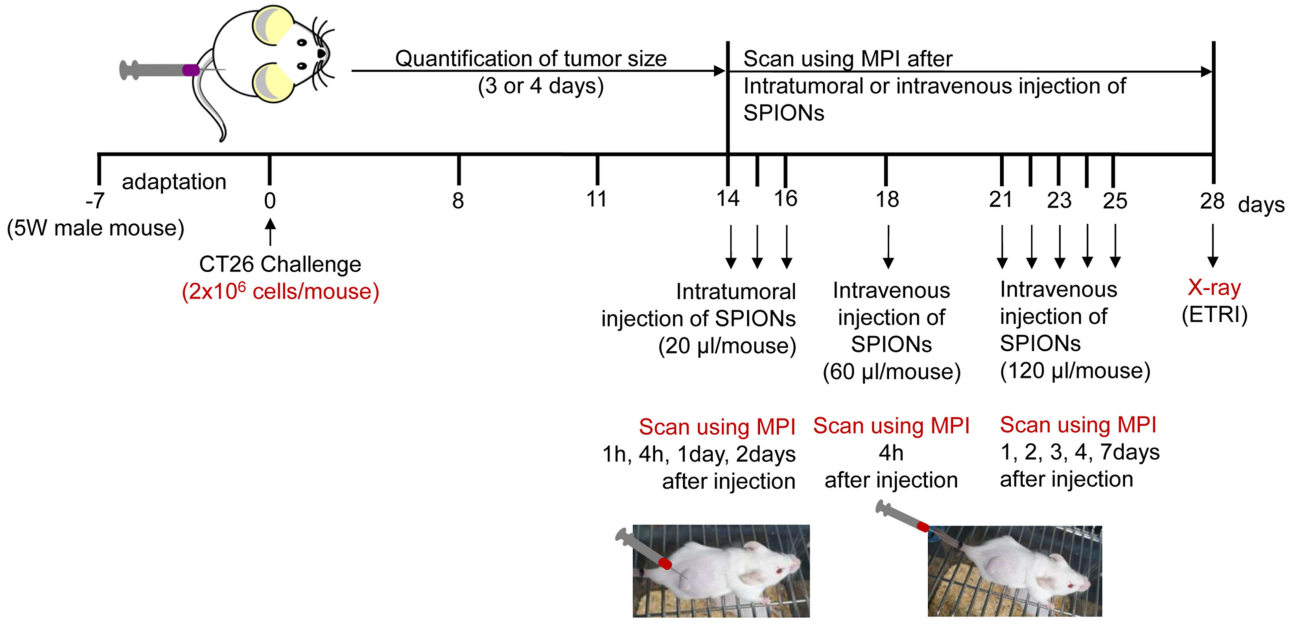

Figure 1 Experimental timeline of CT26 challenge and nanoparticle injection. CT26 tumor-bearing BALB/c mice were injected intratumorally with superparamagnetic iron oxide nanoparticles (SPIONs; 20 µL/mouse) at each time point and scanned using magnetic particle imaging (MPI) at 1 h, 4 h, 1 d, and 2 d post-injection. Another group of CT26 tumor mice were injected intravenously with SPIONs (60 or 120 µL/mouse) at each time point and scanned using MPI at 4 h and 1, 2, 3, 4, 7, and 18 d post-injection.
Abbreviation: ETRI, Electronics and Telecommunications Research Institute.

Prussian Blue Staining for Tumor Histology of SPOINs

After sacrificing the experimental animals (both the intratumoral and the intravenous C57BL/6 tumor mice), tumor tissues were extracted and fixed in 10% formalin neutral buffer solution for 24 h, embedded in paraffin wax, and sectioned for histological examination at 6 µm. Prussian blue iron stain was used to detect the accumulation of SPIONs inside the tumor tissues. Prussian blue and nuclear fast red staining were carried out according to the manufacture's protocol (VB-3009, VitroVivo Biotech, Rockville, MD, USA). Briefly, slides were de-paraffinized in xylene, re-hydrated in serial alcohol dilutions from 100%, 95%, 90%, 80% 70% to tap water. A mixture of equal volumes 5% potassium ferricyanide solution and 5% hydrochloric acid solution was prepared and used to stain slides for 30 min. The slides were then washed in distilled water and counter-stained with nuclear fast red solution for 5 min. Subsequently, the slides were dehydrated through a graded ethanol series, cleared in xylene, and cover-slipped with Permount (Fisher Scientific, Pittsburgh, PA, USA). Light photo micrographic images were acquired using an Olympus CX23 microscope (Olympus Inc., Tokyo, Japan).

Biodistribution Analysis to Confirm the in vivo Stability of SPIONs

The quantitative biodistribution of SPIONs visualized using PoCT-MPI was investigated using the intravenous mice model as described earlier. The C57BL/6 mice were sacrificed to measure the SPIONs accumulated in the tumor and liver tissue at the afore-mentioned time points after SPION injection. The density of SPION accumulation in each tissue was measured using 1D MPI (Mag-Solution Co., Daejeon, Korea).

Results

Establishment of Two Syngeneic Tumor Mouse Models

CT26 and MC38 syngeneic tumor mouse models were constructed to visualize SPIONs within tumor sites; a timeline of the experiments is summarized in Figures 1 and S1. Despite the increased size of the tumor, there was no significant change in the weight of the experimental BALB/c (Figure 2) and C57BL/6 mice (Figure S2). Tumor volume was measured every three days from day 8 to day 14 for BALB/c mice (Figure 3A) and from day 7 to day 14 for C57BL/6 mice (Figure S3). No change was observed in the tumor size of the PBS group. The mean tumor volume in the

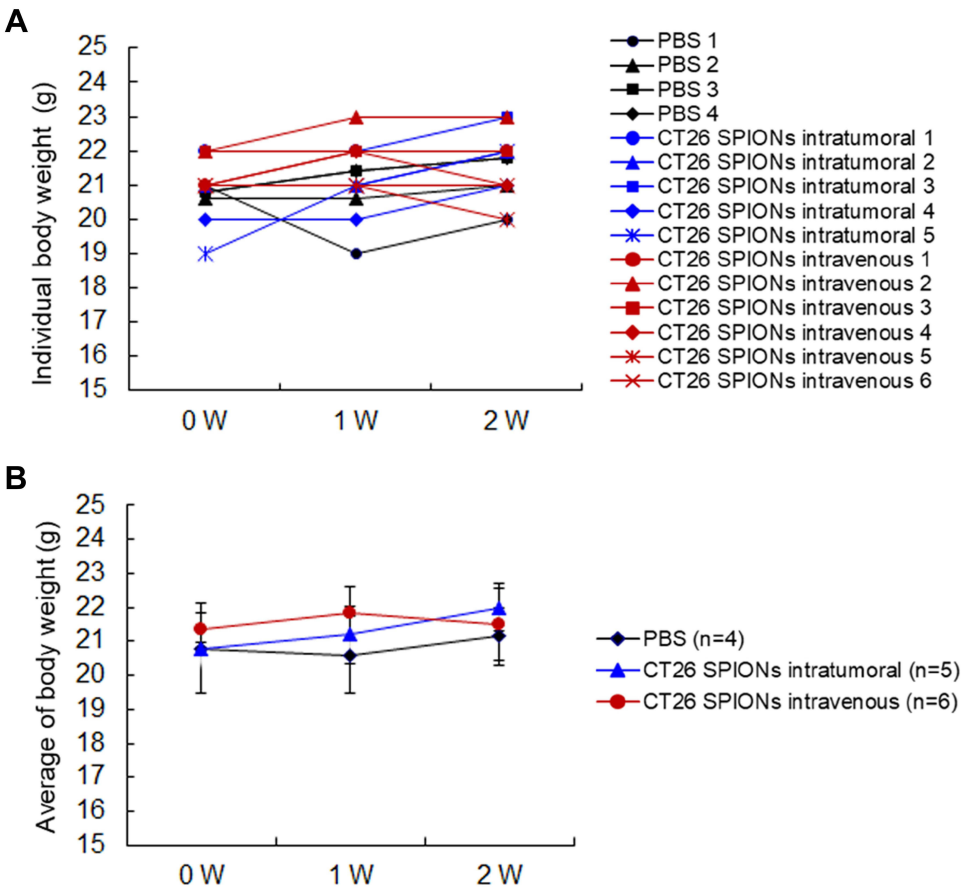

Figure 2 Body weights of male BALB/c mice injected intratumorally or intravenously with superparamagnetic iron oxide nanoparticles (SPIONs) following CT26 challenge. (**A**) Individual and (**B**) average body weights of mice injected with CT26 tumor cells. The body weight was measured every 7 d post-CT26 challenge. PBS group, n = 4; Intratumoral group, n = 5; Intravenous group, n = 6.

intratumoral group was 65.2 ± 8.2 mm^3 after 8 d, 124.3 ± 16.0 mm^3 after 11 d, and 225.3 ± 28.9 mm^3 after 14 d (Figure 3B). The mean tumor volume in the intravenous group was 61.2 ± 8.7 mm^3 after 8 d, 119.1 ± 20.2 mm^3 after 11 d, and 221.1 ± 35.2 mm^3 after 14 d (Figure 3B). The mean tumor volumes between the intratumoral and intravenous groups were similar on day 14 (Figures 3C, and S3C). Figures 3D and S3D show the images of excised tumors after SPION administration and PoCT-MPI scan.

Tumor Visualization in the Intratumoral Group Using PoCT-MPI

Following direct injection into the tumor lesion, SPIONs were effectively visualized using PoCT-MPI. After the intratumoral injection of 20 µL SPIONs, 3D MPI scanning was performed at 1 and 4 h to visualize the tumor, and subsequent experiments were carried out as scheduled (Figure 4A). The SPION signal appeared 1 h after intratumoral SPION administration and persisted until 2 d without any apparent decrease in signal intensity (Figure 4B and C). Moreover, intratumoral injection of SPIONs did not lead to their accumulation in the liver or any other organs (Figure 4). Additionally, 1, 3, and 5 d after intratumoral injection, the MC38 syngeneic tumor model exhibited similar results (Figure S4). Hence, intratumoral injection of SPIONs can detect solid tumors without the use of radioisotopes.

Tumor Visualization in the Intravenous Group Using PoCT-MPI

In the intravenous group of the CT26 syngeneic model, 4 h after intravenous administration, SPIONs were visualized and found to be accumulated in the liver, not at the tumor site (Figure 5A). Subsequently, SPIONs were visualized in vivo in the tumor lesions as well as in the liver on day 1 following an intravenous tail vein injection (Figure 5A). Moreover, SPION signals appeared on day 1 and persisted up to day 7 after intravenous administration (Figure 5A).

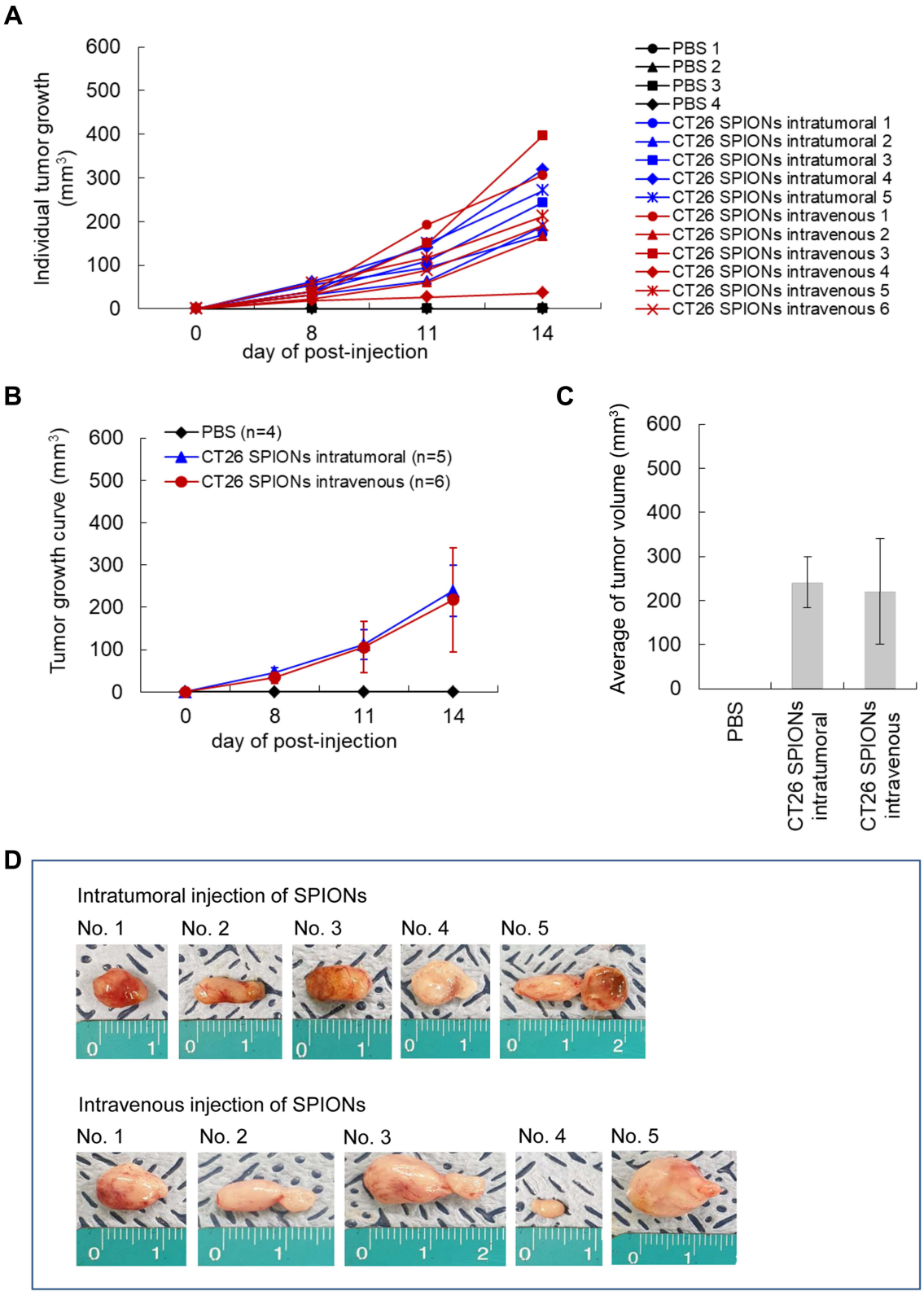

Figure 3 Development of CT26-derived tumors in a BALB/c syngeneic mouse tumor model. (**A**) Individual tumor growth. Tumor volume was measured every three days from day 8 to day 14. (**B**) Average tumor growth curve, PBS group, n = 4; Intratumoral group, n = 5; Intravenous group, n = 6. (**C**) Average tumor volume on day 14 post-CT26 inoculation, and (**D**) images of tumors excised after the superparamagnetic iron oxide nanoparticles (SPIONs) were injected; magnetic particle imaging (MPI) scanning was completed according to the schedule shown in. Figure 1

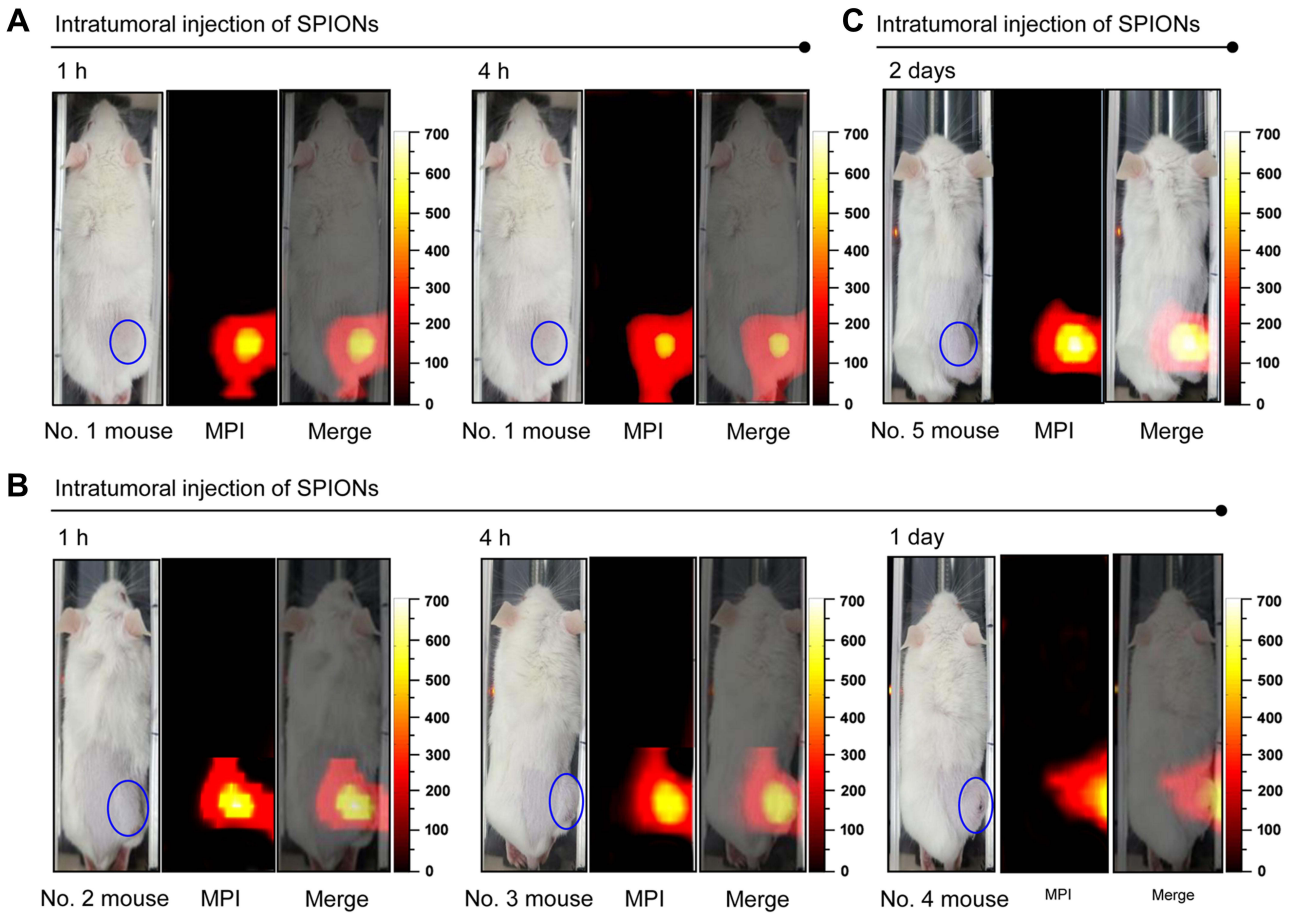

Figure 4 Magnetic particle imaging (MPI) 3D scanning of CT26-inoculated BALB/c mice with superparamagnetic iron oxide nanoparticles (SPIONs; 20 μL/mouse) injected directly into tumor lesions. The SPIONs intensity was characterized by PoCT-MPI images 1 h, 4 h (**A**), 1 d (**B**), 2 d (**C**) after injection of SPIONs into tumor-bearing mice (n = 5). Blue circles indicate the tumor regions.

Additionally, following 1D scanning on day 4, we confirmed that the MPI appeared as two peaks corresponding to the SPION signals detected in the liver and tumor (Figure 5A). Figure 5B shows the results from the other mice. Two SPION signal peaks were detected upon 1D scanning on day 3, and their location in the liver and tumor was confirmed through 3D scanning. Similarly, the measured signal of SPIONs was maintained for up to 7 d (Figure 5B). Eighteen days after intravenous administration, the signal disappeared only at the tumor site, not in the liver (Figure 5B). Figure 5C shows the results of the "vehicle group" injected with PBS, for which no SPION signal was detected, as expected. Moreover, we performed 3D serial sinograms of intratumorally or intravenously injected mice, the results of which were similar to those obtained using the PoCT-MPI technique. Additionally, 4 h and 1, 3, and 5 d after intravenous injection, the MC38 syngeneic tumor model exhibited similar results (Figure S5). On day 4 after the injection of SPIONs, their anatomical position was confirmed by matching the results with the X-ray image (Figure S6). We also confirmed the presence of SPIONs in the excised tumor tissues from MC38-inoculated C57BL/6 mice of both intratumoral and intravenous models via Prussian blue iron staining (Figure S7). These results indicated that intravenous SPION administration could measure systemic solid tumors without the use of radioisotopes.

Confirmation of the in vivo Stability of SPIONs

The biodistribution of SPIONs was examined to confirm their in vivo stability. After the organs were isolated and homogenized, biodistribution in the liver, spleen, heart, brain, colon, kidney, stomach, and lungs was measured using 1D MPI. As shown in Figure 6A, the biodistribution graph of SPIONs showed for comparison of quantitative amplitude values by SPIONs between blood and several organs. A significant difference was detected between the biodistribution in

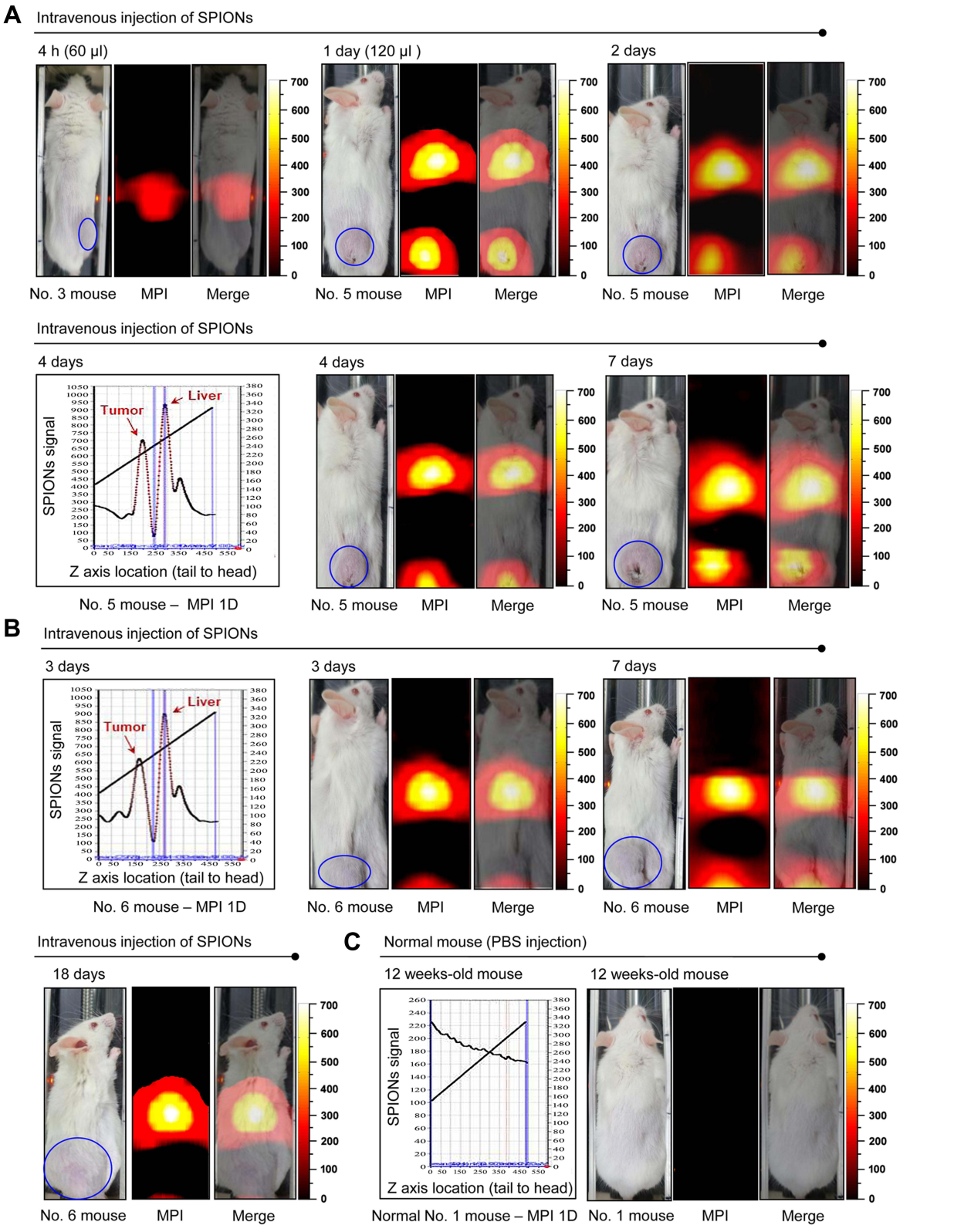

Figure 5 Magnetic particle imaging (MPI) 3D scanning of CT26-inoculated mice administered through the lateral tail veins with superparamagnetic iron oxide nanoparticles (SPIONs). (**A**) PoCT-MPI images were obtained 4 h (60 μL) and 1, 2, 4, and 7 d (120 μL) post-SPION injection. Additionally, the 1D MPI on day 4 appeared as two peaks corresponding to the SPION signals detected in the liver and tumor. (**B**) Images obtained 3, 7, and 18 d (120 μL) post-administration. The 1D MPI on day 3 appeared as two peaks corresponding to the SPION signals detected in the liver and tumor. Blue circles in (**A** and **B**) indicate the tumor regions. (**C**) Normal mouse (vehicle group) injected intravenously with PBS was used as a negative control.

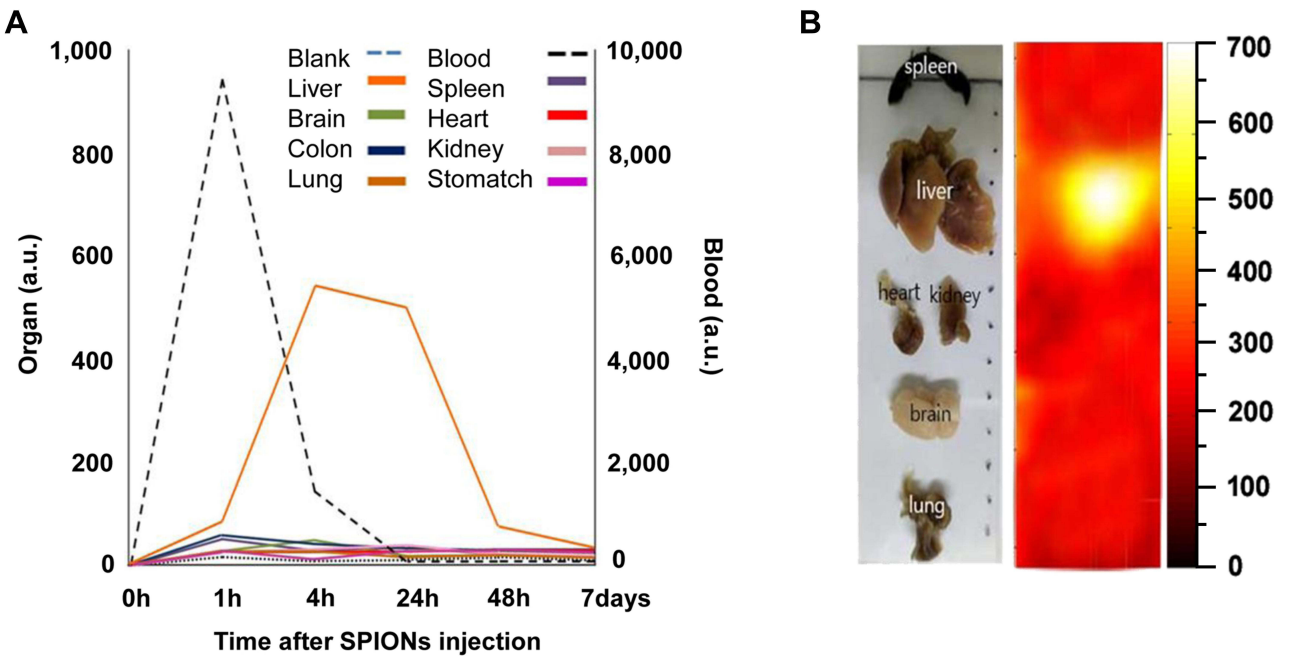

Figure 6 Quantitative estimation of SPIONs acquired from various mouse organs. (**A**) Quantitative level of SPIONs at time points using 1D MPI. Biodistribution was measured in the liver, spleen, heart, brain, colon, kidney, stomach, and lungs using 1D MPI after the organs were isolated and homogenized. (**B**) PoCT-MPI scan (right) and corresponding photograph of major organs (left; spleen, liver, heart, kidney, brain, lungs) excised from mice 4 h post SPION injection.

the blood and liver. The blood showed the largest peak 1 h after injection of SPIONs into the tail vein (amplitude; au = 9672). However, this signal decreased continuously and sharply beginning 4 h after SPION injection with no signal detected after 24 h. Meanwhile, in the liver, the signal began to appear 1 h after injection, peaked at 4 h (amplitude; au = 569), and decreased continuously after 24 h (Figure 6A). To reconfirm the amplitude value for each organ detected through 1D MPI at 4 h after SPIONs injection, the signal of SPIONs was confirmed in the same organs using 3D PoCT-MPI (Figure 6B). The spleen, liver, heart, kidney, brain, and lung were imaged 4 h after tail vein injection of SPIONs using PoCT-MPI. Results indicated that SPION signals were detected only in the liver (Figure 6B). Based on these results, it was confirmed that the intravenous injection of SPIONs did not affect organs other than the liver.

Discussion

We recently proposed a compact and low-power 3D MPI device, PoCT-MPI, which uses a hybrid-type selection field and an FMMD sensor.[23] The present study was conducted to confirm the biological applicability of this newly developed PoCT-MPI technology. We succeeded in imaging the tumor lesions in the CT26 syngeneic mouse tumor model, imaging 5 μg (Fe) of SPIONs with diameters of 50 nm using PoCT-MPI with a spatial resolution of 5.4×5.4 × 15 mm for the x, y, and z-axes, respectively. A study conducted by another research group[24] found that the lowest detection limit for Resovist that could be imaged using an MPI-tailored SPIO tracer (LodeSpin Labs., Seattle, WA, USA) was 3 ng (Fe). The same research group reported that the spatial resolution in the x-, y-, and z-axes was 1×1 × 0.7 mm, respectively. This difference is likely due to the lower magnetic power of PoCT-MPI. Therefore, application of an additional powerful and permanent magnet to PoCT-MPI should, theoretically, increase the gradient field and improve the resolution in the x-, y-, and z-axes, commensurable with that of the traditional MPI.

Herein, PoCT-MPI was applied to a pathological syngeneic mouse tumor model to explore the final goal of our study. When the SPIONs in the internal organ (tumor) are exposed to the appropriate external alternating magnetic field, the magnetic energy dissipation caused by internal Neel fluctuations of the SPIONs can generate heat and increase the temperature inside the tumor.[8,9,25] Indeed, magnetic fluid hyperthermia (MFH) can improve the effectiveness of cancer treatment when applied in combination with various other treatments, such as chemotherapy.[26,27] Our study aimed to determine whether SPIONs injected into blood vessels could accumulate within the tumor tissues and whether PoCT-MPI can effectively visualize them. To create

a tumor model, male BALB/c mice were subcutaneously inoculated with colon cancer CT26 cells. The trial period was limited to 17 d after tumor cell inoculation since skin necrosis was observed following excessive tumor growth. We first determined how long the SPIONs were retained following direct injection into the tumor tissue in the intratumoral injection model and whether PoCT-MPI could visualize them. Following direct injection into the tumor tissue, image acquisition was possible for up to 2 d, which defined the period of the current study. Significant changes in the concentration and spread of SPIONs to other organs were not observed (Figure 4). Hence, MFH, which is limited to cancerous tissues, is possible without damaging the surrounding normal tissue, when SPIONs are injected directly into certain cancer tissues.

Next, after administering SPIONs into the tumor animal model through the tail vein, the accumulation of SPIONs in tumor tissues was monitored using PoCT-MPI. SPIONs accumulated in the liver as well as in the tumor tissue. Kupffer cells are liver-resident macrophages lining the walls of the liver sinusoids that contribute to the innate immune response in the liver.[28] Therefore, it is thought that SPIONs injected into the body (through the circulatory system) can accumulate in the liver due to the ability of Kupffer cells to engulf foreign substances.[29] Indeed, the biodistribution study showed that SPIONs injected through the blood vessels were targeted directly to the tumor, with negligible accumulation in major organs (brain, spleen, heart, kidney, and lung), except for the liver (Figure 6). The accumulation of SPIONs in tumor tissue can be explained by the enhanced permeability and retention (EPR) effect, which is the mechanism by which high molecular weight non-targeted foreign substances accumulate in tissues that offer increased vascular permeability, such as at sites of inflammation.[30] The aberrant vascular architecture caused by the excessive production of the vascular permeability factor and lack of lymphatic drainage of the tumor tissue, creates a more enhanced EPR effect.[31–33] Therefore, SPIONs in the circulatory system can considerably accumulate in tumor tissue without the aid of targeting strategies, such as tumor-specific antibody conjugation. As such, we are confident that results from research conducted with preclinical MPI systems will provide valuable guidance for the ongoing development of a whole-body clinical MPI system.

SPIONs are a type of magnetic nanoparticles composed of magnetite (Fe_3O_4) or maghemite (γ-Fe_2O_3) and the size usually ranges from 20 to 150 nm. Because of their superparamagnetic properties, SPIONs have a various applications in MRI, MPI and MFH. Because SPIONs can be conjugated with various molecules, they have a wide range of possible uses. In addition, residual magnetization is not observed in the absence of the external magnetic field; thus, precise remote control over their action is possible. These characteristics of SPIONs indicate their promise in oncological diagnosis and therapy.[34] As shown in this study, MPI can visualize only the SPIONs that are accumulated in cancerous tissue by EPR effect without any aid of targeting strategies. SPIONs also produce precise and uniform heating over a wide temperature range, which can elicit sustained antitumoral immune responses through a variety of mechanisms, such as (1) natural killer cell activation and proliferation, (2) enhanced anticancer activity of dendritic cells and T cells, (3) increased exosome release, (4) MHC (major histocompatibility complex) I upregulation on the tumor cell surface, and (5) increased immune cell permeation into the tumor tissue.[35] Therefore, the development of a device capable of simultaneously performing MFH and MPI using SPIONs could be very promising as a theranostics platform for the simultaneous realization of tumor diagnosis and treatment.

However, the biocompatibility and biosafety of SPIONs are crucial requirements for successful clinical application. Certain SPIONs (ferumoxtran-10, ferumoxides, ferumoxytol, etc.) have been clinically approved for use in the medial field. However, their potential toxicity and biocompatibility remain under discussion.[36] Our biodistribution analysis showed that SPIONs (Synomag-D) administered intravenously were almost completely cleared from major organs within 1 d, except in the liver, from which they were cleared within 4 d. Although the rapid clearing rate of SPIONs does not definitively prove their biosafety, it is expected that cancer diagnosis using MPI can be sufficiently applied in the clinic if a precisely controlled protocol is established.

Most cancers can actively metastasize to other organs, a process that is not random. Metastasis is regulated by several factors, including cancer subtypes, molecular characteristics of cancer cells, and the host immune microenvironment. This pathological process is referred to as "metastatic organotropism."[37] It will, therefore, be of significant interest to apply an organotropic animal model to our study to demonstrate whether our MPI system can detect not only primary cancer but also metastatic cancer.

Conclusion

We have successfully visualized the presence and location of SPIONs in tumor animal models using PoCT-MPI, a low-power compact MPI system. MPI technology has significant advantages in that its coverage has been considerably

expanded due to low production costs and a significant reduction in power demand, differing from conventional medical imaging technologies.[38] However, the following will have to be addressed for future practical use of MPI systems. First, studies on the capacity of suitable SPIONs that can be used in MPI technology are required. Second, pharmacokinetic studies and a review of the biological stability of SPIONs are required. Third, it might be possible to develop conceptually new medical imaging equipment to simultaneously carry out diagnosis and treatment. Theoretically, MPI can not only confirm the presence of SPIONs but also assess SPION accumulation in the desired location through various biochemical processes. Therefore, developing next-generation medical imaging equipment that can be used for simultaneous diagnosis and treatment is promising with regard to the future clinical utility of PoCT-MPI.

Abbreviations

CT, Computed tomography; DMEM, Dulbecco's modified Eagle's medium; EPR, Enhanced permeability and retention; FBS, Fetal bovine serum; MFH, Magnetic fluid hyperthermia; MPI, Magnetic particle imaging; MRI, Magnetic resonance imaging; PBS, Phosphate-buffered saline; PET, Positron emission tomography; PoCT-MPI, Point-of-care testing MPI; SPECT, Single-photon emission computed tomography; SPION, Superparamagnetic iron oxide nanoparticle; WMIC, World molecular imaging congress.

Data Sharing Statement

The datasets used and/or analyzed during the current study are available from the corresponding authors upon reasonable request.

Funding

This research was supported by the Mid-Career Research Program through the National Research Foundation of Korea (2021R1A2C1010951 to DYS) and the Basic Science Research Program through the National Research Foundation of Korea funded by the Ministry of Education (2020R1I1A3066989 to SHL; 2020R1I1A1A01073857 to SRH; 2020R1I1A3073525 to YHK).

Disclosure

This work has been funded by Korea government. The funders had no role in the design of the study; the collection, analysis, or interpretation of the data; the writing of the manuscript; or the decision to submit the manuscript for publication. The authors declare no financial competing interests or non-financial competing interests.

References

1. Gleich B, Weizenecker J. Tomographic imaging using the nonlinear response of magnetic particles. *Nature*. 2005;435(7046):1214–1217. doi:10.1038/nature03808
2. Gaudet JM, Makela AV, Foster PJ. Abstract 1138: non-invasive detection and quantification of tumor-associated macrophage density with magnetic particle imaging. *Cancer Res*. 2019;79(13_Supplement):1138. doi:10.1158/1538-7445.AM2019-1138
3. Lu C, Han L, Wang J, Wan J, Song G, Rao J. Engineering of magnetic nanoparticles as magnetic particle imaging tracers. *Chem Soc Rev*. 2021;50 (14):8102–8146. doi:10.1039/d0cs00260g
4. Bulte JWM. Superparamagnetic iron oxides as MPI tracers: a primer and review of early applications. *Adv Drug Deliv Rev*. 2019;138:293–301. doi:10.1016/j.addr.2018.12.007
5. Talebloo N, Gudi M, Robertson N, Wang P. Magnetic particle imaging: current applications in biomedical research. *J Magn Reson Imaging*. 2020;51(6):1659–1668. doi:10.1002/jmri.26875
6. Saritas EU, Goodwill PW, Croft LR, et al. Magnetic particle imaging (MPI) for NMR and MRI researchers. *J Magn Reson*. 2013;229:116–126.
7. Zheng B, von See MP, Yu E, et al. Quantitative magnetic particle imaging monitors the transplantation, biodistribution, and clearance of stem cells in vivo. *Theranostics*. 2016;6(3):291–301. doi:10.7150/thno.13728
8. Laurent S, Dutz S, Hafeli UO, Mahmoudi M. Magnetic fluid hyperthermia: focus on superparamagnetic iron oxide nanoparticles. *Adv Colloid Interface Sci*. 2011;166(1–2):8–23. doi:10.1016/j.cis.2011.04.003
9. Kumar CS, Mohammad F. Magnetic nanomaterials for hyperthermia-based therapy and controlled drug delivery. *Adv Drug Deliv Rev*. 2011;63 (9):789–808. doi:10.1016/j.addr.2011.03.008
10. Weizenecker J, Gleich B, Rahmer J, Dahnke H, Borgert J. Three-dimensional real-time in vivo magnetic particle imaging. *Phys Med Biol*. 2009;54 (5):L1–L10. doi:10.1088/0031-9155/54/5/L01
11. Tomitaka A, Arami H, Gandhi S, Krishnan KM. Lactoferrin conjugated iron oxide nanoparticles for targeting brain glioma cells in magnetic particle imaging. *Nanoscale*. 2015;7(40):16890–16898. doi:10.1039/C5NR02831K
12. Yu EY, Bishop M, Zheng B, et al. Magnetic particle imaging: a novel in vivo imaging platform for cancer detection. *Nano Lett*. 2017;17 (3):1648–1654. doi:10.1021/acs.nanolett.6b04865

13. Zheng B, Vazin T, Goodwill PW, et al. Magnetic Particle Imaging tracks the long-term fate of in vivo neural cell implants with high image contrast. *Sci Rep*. 2015;5:14055. doi:10.1038/srep14055
14. Chen C, Ge J, Gao Y, et al. Ultrasmall superparamagnetic iron oxide nanoparticles: a next generation contrast agent for magnetic resonance imaging. *Wiley Interdiscip Rev Nanomed Nanobiotechnol*. 2022;14(1):e1740. doi:10.1002/wnan.1740
15. Darson J, Mohan M. Iron oxide nanoparticles and nano-composites: an efficient tool for cancer theranostics; 2022.
16. Subhan MA, Muzibur Rahman M. Recent development in metallic nanoparticles for breast cancer therapy and diagnosis. *Chem Rec*. 2022;22: e202100331. doi:10.1002/tcr.202100331
17. Murar M, Albertazzi L, Pujals S. Advanced optical imaging-guided nanotheranostics towards personalized cancer drug delivery. *Nanomaterials*. 2022;12(3):399. doi:10.3390/nano12030399
18. Yang HM, Park CW, Woo MA, et al. HER2/neu antibody conjugated poly (amino acid)-coated iron oxide nanoparticles for breast cancer MR imaging. *Biomacromolecules*. 2010;11(11):2866–2872. doi:10.1021/bm100560m
19. Siddique S, Chow JCL. Application of nanomaterials in biomedical imaging and cancer therapy. *Nanomaterials*. 2020;10:9. doi:10.3390/nano10091700
20. Chow JCL. 9 - Magnetic nanoparticles as contrast agents in magnetic resonance imaging and radiosensitizers in radiotherapy. In: Hussain CM, Patankar KK, editors. *Fundamentals and Industrial Applications of Magnetic Nanoparticles*. Woodhead Publishing; 2022:291–316.
21. Hong H, Krause HJ, Sohn S, et al. In situ measurement of superoxide and hydroxyl radicals by frequency mixing detection technique. *Anal Biochem*. 2014;447:141–145. doi:10.1016/j.ab.2013.11.009
22. Kim CB, Park SJ, Jeong JC, et al. Construction of 3D-rendering imaging of an ischemic rat brain model using the planar FMMD technique. *Sci Rep*. 2019;9(1):19050. doi:10.1038/s41598-019-55585-x
23. Choi SM, Jeong JC, Kim J, et al. A novel three-dimensional magnetic particle imaging system based on the frequency mixing for the point-of-care diagnostics. *Sci Rep*. 2020;10(1):11833. doi:10.1038/s41598-020-68864-9
24. Yu EY, Chandrasekharan P, Berzon R, et al. Magnetic particle imaging for highly sensitive, quantitative, and safe in vivo gut bleed detection in a murine model. *ACS nano*. 2017;11(12):12067–12076. doi:10.1021/acsnano.7b04844
25. Prasad NK, Rathinasamy K, Panda D, Bahadur D. Mechanism of cell death induced by magnetic hyperthermia with nanoparticles of γ-MnxFe2–xO3 synthesized by a single step process. *J Mater Chem*. 2007;17(48):5042–5051. doi:10.1039/b708156a
26. Di Corato R, Bealle G, Kolosnjaj-Tabi J, et al. Combining magnetic hyperthermia and photodynamic therapy for tumor ablation with photo-responsive magnetic liposomes. *ACS nano*. 2015;9(3):2904–2916. doi:10.1021/nn506949t
27. Gogoi M, Jaiswal MK, Sarma HD, Bahadur D, Banerjee R. Biocompatibility and therapeutic evaluation of magnetic liposomes designed for self-controlled cancer hyperthermia and chemotherapy. *Integr Biol*. 2017;9(6):555–565. doi:10.1039/C6IB00234J
28. Sharifi S, Seyednejad H, Laurent S, Atyabi F, Saei AA, Mahmoudi M. Superparamagnetic iron oxide nanoparticles for in vivo molecular and cellular imaging. *Contrast Media Mol Imaging*. 2015;10(5):329–355.
29. Zhang YN, Poon W, Tavares AJ, McGilvray ID, Chan WCW. Nanoparticle-liver interactions: cellular uptake and hepatobiliary elimination. *J Control Release*. 2016;240:332–348. doi:10.1016/j.jconrel.2016.01.020
30. Torchilin V. Tumor delivery of macromolecular drugs based on the EPR effect. *Adv Drug Deliv Rev*. 2011;63(3):131–135. doi:10.1016/j.addr.2010.03.011
31. Alexiou C, Jurgons R, Schmid RJ, et al. Magnetic drug targeting–biodistribution of the magnetic carrier and the chemotherapeutic agent mitoxantrone after locoregional cancer treatment. *J Drug Target*. 2003;11(3):139–149. doi:10.3109/1061186031000150791
32. Prabhakar U, Maeda H, Jain RK, et al. Challenges and key considerations of the enhanced permeability and retention effect for nanomedicine drug delivery in oncology. *Cancer Res*. 2013;73(8):2412–2417. doi:10.1158/0008-5472.CAN-12-4561
33. Maeda H, Nakamura H, Fang J. The EPR effect for macromolecular drug delivery to solid tumors: improvement of tumor uptake, lowering of systemic toxicity, and distinct tumor imaging in vivo. *Adv Drug Deliv Rev*. 2013;65(1):71–79. doi:10.1016/j.addr.2012.10.002
34. Dulinska-Litewka J, Lazarczyk A, Halubiec P, Szafranski O, Karnas K, Karewicz A. Superparamagnetic iron oxide nanoparticles-current and prospective medical applications. *Materials*. 2019;12:4. doi:10.3390/ma12040617
35. Toraya-Brown S, Fiering S. Local tumour hyperthermia as immunotherapy for metastatic cancer. *Int J Hyperth*. 2014;30(8):531–539. doi:10.3109/02656736.2014.968640
36. Natarajan P, Tomich JM. Understanding the influence of experimental factors on bio-interactions of nanoparticles: towards improving correlation between in vitro and in vivo studies. *Arch Biochem Biophys*. 2020;694:108592. doi:10.1016/j.abb.2020.108592
37. Chen W, Hoffmann AD, Liu H, Liu X. Organotropism: new insights into molecular mechanisms of breast cancer metastasis. *NPJ Precis Oncol*. 2018;2(1):4. doi:10.1038/s41698-018-0047-0
38. Panagiotopoulos N, Duschka RL, Ahlborg M, et al. Magnetic particle imaging: current developments and future directions. *Int J Nanomedicine*. 2015;10:3097–3114. doi:10.2147/IJN.S70488